A Highly Accurate Current LED Lamp Driver With Removal of Low-Frequency Flicker Using Average Current Control Method

Hyun-A Ahn, *Student Member, IEEE*, Seong-Kwan Hong, *Member, IEEE*, and Oh-Kyong Kwon, *Member, IEEE*

***Abstract*—This paper presents an average current control method for a light-emitting diode (LED) lamp driver that achieves a highly accurate current and removes low-frequency light flicker. The proposed LED lamp driver accurately maintains an average LED forward current by precisely adjusting the duration of the on- and off-times of the LED lamp driver. It also removes the low-frequency flicker by regulating the LED forward current without being affected by the low-frequency component of the ac line voltage. In addition, it reduces power consumption by eliminating the necessity of a high-voltage sensor or a high-side resistor, which causes conduction loss. The proposed average current controller was fabricated using a 0.18 μm bipolar, complementary metal-oxide-semiconductor, and double diffused metal-oxide-semiconductor process technology. The measurement results of the proposed LED lamp driver show that the variation in the average LED forward current is less than 0.6%, and the light flicker below 120 Hz is completely removed. In addition, the measured maximum power efficiency and power factor of the proposed LED lamp driver are 89.22% and 0.93, respectively.**

***Index Terms*—AC–DC power conversion, current control, light-emitting diode (LED), lighting, driver circuits.**

I. Introduction

RECENTLY, light-emitting diodes (LEDs) have been increasingly used as lighting devices due to their high power efficiency, long lifetime, and environmental friendliness [1], [2]. The use of LEDs helps us to alleviate global warming because high-efficiency lighting reduces carbon emissions. Moreover, since regulations for the use of incandescent lamps are globally strengthened, LED lamps will rapidly dominate the market for lighting devices [3], [4].

To use LEDs as a lighting lamp, an LED lamp driver is needed to supply stable power to LEDs and to accurately control the luminance of LEDs. Since the luminance of LEDs is determined by the average current flowing through LEDs, a method of accurately controlling the average LED current is necessary to acquire accurate luminance in the LED lamp driver. In addition, the LED lamp driver requires the characteristics of high power efficiency, high power factor, low system cost, long lifetime, and low light flicker, where the light flicker is mainly induced by ac main power sources.

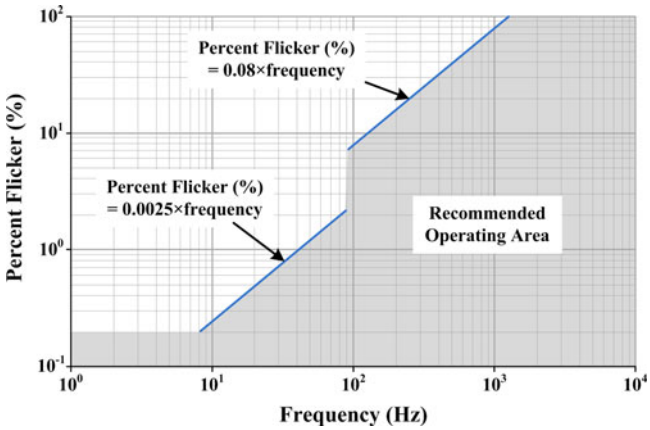

Fig. 1. Recommended operating area of percent flicker according to frequency [9].

In lighting applications, luminance accuracy depends on the deviation of luminance between the LED lamps, and the variation in luminance of a single LED lamp. Deviation of luminance is mainly caused by variations in both the forward voltage of the LED and the inductance of the inductor or transformer. Since commercial LEDs and inductors provide an allowable deviation of 20%, an LED lamp driver should be carefully designed with the consideration of such a deviation in order to accurately control the luminance. On the other hand, the variation in luminance is mainly induced by an ac line voltage of 110 V or 220 V. According to medical research, such variation leads to low-frequency light flicker, which can be harmful to human health [5]–[8]. Thus, the IEEE standard 1789-2015 in high brightness LEDs was established to mitigate health risks to viewers [9]. The light flicker, which is defined as a variation in lamp luminance according to time [9], can be quantified as a percent flicker, which is expressed as

$$\text{Percent flicker}(\%) = \frac{L_{\max} - L_{\min}}{L_{\max} + L_{\min}} \times 100 \qquad (1)$$

Manuscript received July 12, 2017; revised September 27, 2017 and November 2, 2017; accepted December 11, 2017. Date of publication December 15, 2017; date of current version July 15, 2018. Recommended for publication by Associate Editor X. Wu. *(Corresponding author: Oh-Kyong Kwon.)*

The authors are with the Department of Electronic Engineering, Hanyang University, Seoul 04763, South Korea (e-mail: ffaha@hanyang.ac.kr; seongkhong@hanyang.ac.kr; okwon@hanyang.ac.kr).

Color versions of one or more of the figures in this paper are available online at http://ieeexplore.ieee.org.

Digital Object Identifier 10.1109/TPEL.2017.2783921

See http://www.ieee.org/publications_standards/publications/rights/index.html for more information.

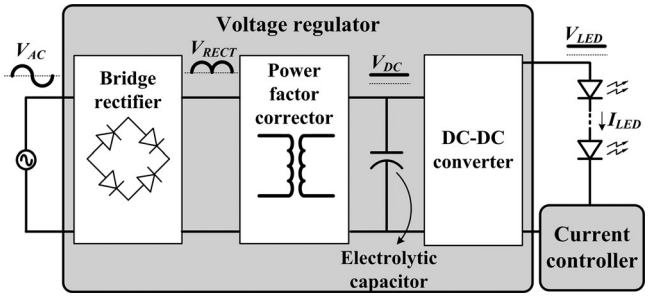

Fig. 2. Block diagram of a typical two-stage LED lamp driver.

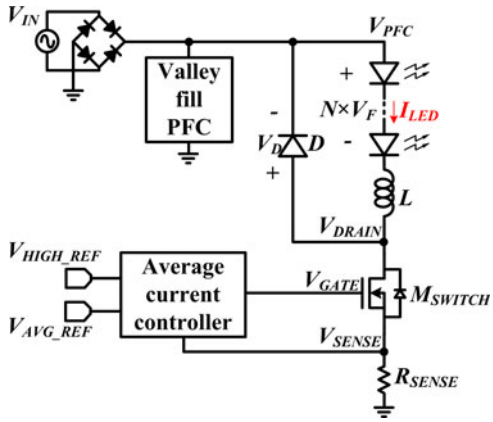

Fig. 3. Proposed LED lamp driver using the ACC method.

where $L_{\max}$ and $L_{\min}$ are the maximum and minimum luminance, respectively. Fig. 1 shows the recommended operating area for percent flicker according to frequency (f), indicating that the percent flicker should be less than $0.0025 \times f$ or $0.08 \times f$ depending on whether f is below or above 90 Hz, respectively. Since the light flicker below 90 Hz, called visible flicker, can be recognized with human eyes, it is severely harmful to human health. Therefore, the percent flicker below 90 Hz is more strictly regulated than that above 90 Hz; thus, recent LED lamp drivers have been developed to comply with the recommended standard of percent flicker [10]–[15].

Fig. 2 shows a typical two-stage LED lamp driver, which consists of a voltage regulator for providing a regulated voltage to the LEDs and a current controller for controlling the luminance of LEDs. In the voltage regulator, the bridge rectifier rectifies the ac main voltage, the power factor corrector (PFC) increases the power factor, and the dc–dc converter regulates the voltage provided to the LEDs for high power efficiency. However, a transformer-based PFC increases the system cost, and a bulky electrolytic capacitor decreases the lifetime of the LED lamp driver because the lifetime of the electrolytic capacitor is much shorter than that of LEDs [16]. In the current controller, several control methods, such as pulse-width modulation [17], [18], pulse-amplitude modulation [19], hysteretic current control [20], and peak current control [21], can be adopted to control the luminance of LEDs.

To improve the performance and reduce the system cost of LED lamp drivers, several current control methods with a simple structure of the LED lamp driver have been studied [22]–[25]. In [22], a step-down buck converter with a constant off-time control method was employed for a simple LED lamp driver to reduce the system size by removing a bulky electrolytic capacitor and directly driving the LEDs from an ac outlet source for a high power factor. However, this LED lamp driver had a large current ripple, which was estimated to have a percent flicker of 100% at low frequency (double the ac line frequency). Moreover, the average LED forward current varied according to the number of LEDs, the inductance of the converter, and the LED forward voltage; thereby, the luminance of LEDs could become inaccurate. The adaptive off-time (AOT) control method in [23] accurately controlled the LED forward current, but required a high-voltage sensor to sense the high voltage at the input of the LED string, thereby increasing the system cost and controller size. Another AOT control method in [24] and [25] employed a low-side resistor to accurately control the LED forward current by sensing the highest and lowest LED forward currents. However, it needed a blanking time before sampling the lowest LED forward current to avoid the overshoot current, caused by turning ON the main power switch. Due to the delay of the blanking time, an LED forward current sampler inaccurately sensed the lowest LED forward current; thus, the LED lamp driver could not accurately control the luminance of the LEDs. Moreover, this control method used a fixed blanking time and had a varying slope of the LED forward current due to an ac main input voltage with a low frequency of 50 or 60 Hz; thus, the lowest LED forward current level varies with double the ac line frequency. Consequently, the low-frequency light flicker could not be removed.

In this paper, an average LED current control method is proposed to achieve a high current accuracy and remove low-frequency light flicker, while maintaining the high power efficiency and power factor of an LED lamp driver without using an electrolytic capacitor. The proposed LED lamp driver using the average current control (ACC) method enhances the accuracy of the LED forward current by precisely adjusting the duration of the on- and off-times of the LED lamp driver without using a high-voltage sensor or high-side resistor. It also removes the low-frequency flicker by regulating the LED forward current without being affected by the low frequency of the ac line voltage. In Section II, the proposed ACC method is theoretically analyzed. Sections III and IV, respectively, explain the operation and circuit implementation of the proposed LED lamp driver using an ACC method. In Section V, the experimental results of the proposed LED lamp driver are presented with a detailed analysis. Finally, the conclusions are given in Section VI.

II. Proposed LED Driver Using the ACC Method

A. Structure of the Proposed LED Lamp Driver

Fig. 3 shows the proposed LED lamp driver using an ACC method for accurately controlling the LED forward current. The proposed LED lamp driver, which employs a floating buck converter structure, consists of a bridge rectifier, a valley-fill PFC, an LED string, an inductor with an inductance of L, a freewheeling diode (D) with a forward voltage of V_D, a power

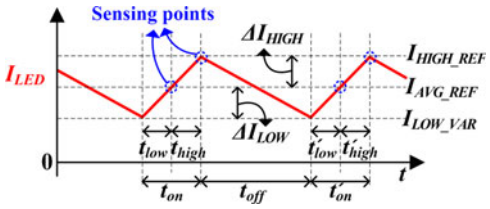

Fig. 4. Conceptual waveform of $I_{\rm LED}$ in the proposed LED lamp driver using the ACC method.

switch ($M_{\rm SWITCH}$), a sensing resistor ($R_{\rm SENSE}$), and an average current controller.

The bridge rectifier uses an ac line voltage ($V_{\rm IN}$) as an input to the LED lamp driver and supplies a rectified voltage ($V_{\rm PFC}$) to an LED string consisting of N LEDs, each of which has a forward voltage of V_F.

The valley-fill PFC is used as a power buffer that supplies power to the LED string when $V_{\rm IN}$ is less than half-peak $V_{\rm IN}$, thus, maintaining a high power factor.

The inductor is energized or de-energized so as to control the LED forward current ($I_{\rm LED}$), whose slope is determined according to $V_{\rm PFC}$, V_D, $N \times V_F$, and the drain voltage of $M_{\rm SWITCH}$ ($V_{\rm DRAIN}$). It is energized or de-energized depending on whether $M_{\rm SWITCH}$ is turned ON or OFF, respectively.

The average current controller generates a gate voltage of $M_{\rm SWITCH}$ ($V_{\rm GATE}$) to control the duration of the on- and off-times of $M_{\rm SWITCH}$ using the sensed voltage across $R_{\rm SENSE}$ ($V_{\rm SENSE}$) and the reference voltages ($V_{\rm HIGH\_REF}$ and $V_{\rm AVG\_REF}$).

B. Proposed ACC Method

In the proposed LED lamp driver, the ACC method is realized to accurately regulate an average $I_{\rm LED}$ to a target average current level by adjusting the durations of the on- and off-times of the LED lamp driver. In addition, it removes the low-frequency flicker without being affected by the blanking time.

Fig. 4 shows the conceptual waveform of $I_{\rm LED}$ of the proposed LED lamp driver using the ACC method. $I_{\rm HIGH\_REF}$ and $I_{\rm AVG\_REF}$ are the fixed levels of the highest $I_{\rm LED}$ and target average $I_{\rm LED}$, which are determined by $V_{\rm HIGH\_REF}/R_{\rm SENSE}$ and $V_{\rm AVG\_REF}/R_{\rm SENSE}$, respectively. $\Delta I_{\rm HIGH}$ is the difference between $I_{\rm HIGH\_REF}$ and $I_{\rm AVG\_REF}$. $I_{\rm LOW_VAR}$is the variable level of the lowest $I_{\rm LED}$, and it varies according to $t_{\rm on}$ and $t_{\rm off}$, which are defined as the durations of the on- and off-times of $M_{\rm SWITCH}$, respectively. $t_{\rm on}$ is divided into $t_{\rm low}$ and $t_{\rm high}$, which are the durations of $I_{\rm LED}$ from $I_{\rm LOW\_VAR}$ to $I_{\rm AVG\_REF}$ and from $I_{\rm AVG\_REF}$ to $I_{\rm HIGH\_REF}$, respectively. $\Delta I_{\rm LOW}$ is the difference between $I_{\rm AVG\_REF}$ and $I_{\rm LOW\_VAR}$.

When $M_{\rm SWITCH}$ is turned ON during $t_{\rm on}$, $I_{\rm LED}$ flows through $M_{\rm SWITCH}$ to ground, and the inductor is energized with a positive slope of $I_{\rm LED}$, which is expressed as

$$\frac{dI_{\rm LED}}{dt_{\rm on}} = \frac{V_{\rm PFC} - N \times V_F - V_{\rm DRAIN}}{L}. \tag{2}$$

When $M_{\rm SWITCH}$ is turned OFF during $t_{\rm off}$, $I_{\rm LED}$ flows through D, and the inductor is de-energized with a negative slope of $I_{\rm LED}$, which is expressed as

$$\frac{dI_{\rm LED}}{dt_{\rm off}} = \frac{-V_D - N \times V_F}{L}. \tag{3}$$

In the hysteretic waveform of $I_{\rm LED}$ of Fig. 4, the average value of $I_{\rm LED}$ is equal to $I_{\rm AVG\_REF}$ when $I_{\rm LOW\_VAR}$ satisfies the following equation:

$$\frac{1}{T}\int_0^T I_{\rm LED} dt = \frac{I_{\rm HIGH\_REF} + I_{\rm LOW\_VAR}}{2} = I_{\rm AVG\_REF} \tag{4}$$

where T is the duration of one switching period ($t_{\rm on}$ plus $t_{\rm off}$). From (4)

$$\begin{aligned} I_{\rm LOW\_VAR} &= 2I_{\rm AVG\_REF} - I_{\rm HIGH\_REF} \\ &= I_{\rm AVG\_REF} - \Delta I_{\rm HIGH}. \end{aligned} \tag{5}$$

From (5), $I_{\rm AVG\_REF} - I_{\rm LOW\_VAR}$ is equal to $\Delta I_{\rm HIGH}$; thus, $\Delta I_{\rm LOW}$ should be equal to $\Delta I_{\rm HIGH}$ to make the average value of $I_{\rm LED}$ equal to $I_{\rm AVG\_REF}$. Consequently, $t_{\rm low}$ should be equal to $t_{\rm high}$, since the slope of $I_{\rm LED}$ is a constant, as expressed in (2).

To make $t_{\rm low}$ equal to $t_{\rm high}$, the proposed average current controller senses the crossing points of $I_{\rm LED}$ with $I_{\rm HIGH\_REF}$ and $I_{\rm AVG\_REF}$ during $t_{\rm on}$ and measures $t_{\rm low}$ and $t_{\rm high}$. When $t_{\rm low}$ is shorter than $t_{\rm high}$, the proposed controller increases $t_{\rm off}$ to extend $t_{\rm low}$ of the next $t'_{\rm on}$ ($t'_{\rm low}$). When $t_{\rm low}$ is longer than $t_{\rm high}$, the proposed controller decreases $t_{\rm off}$ to reduce the subsequent $t'_{\rm low}$. Through the above control process, $t_{\rm low}$ is gradually adjusted to be equal to $t_{\rm high}$, and the proposed LED lamp driver then starts operating in the steady state.

Therefore, using the proposed ACC method, the average $I_{\rm LED}$ is accurately regulated regardless of variation in the slope of $I_{\rm LED}$, which is caused by variation in V_F or L; thus, the luminance of the LED lamp driver can be accurately controlled. In addition, although $V_{\rm PFC}$ varies due to variation in $V_{\rm IN}$ with a low frequency of 60 Hz, the proposed average current controller also accurately controls $I_{\rm LED}$, resulting in removal of low-frequency flicker, which will be explained in detail in Section III-C.

III. Operation of the Proposed LED Lamp Driver

A. Architecture of the Proposed Average Current Controller

Fig. 5 shows the schematic of the proposed LED lamp driver with the average current controller. The proposed average current controller consists of a time measurement block, a time-to-voltage converter, an on- and off-time controller, and a block for a voltage regulator and a bias generator.

The time measurement block compares $V_{\rm SENSE}$ with $V_{\rm HIGH\_REF}$ and $V_{\rm AVG\_REF}$, and measures $t_{\rm high}$ and $t_{\rm low}$ of $I_{\rm LED}$, respectively, as described in Section II-B. Its outputs (Q_1 and Q_2) are then activated during $t_{\rm high}$ and $t_{\rm low}$, respectively. A leading-edge blanking (LEB) block generates a blanking signal ($V_{\rm LEB}$) to prevent the overshoot current occurring when $M_{\rm SWITCH}$ is turned ON as $V_{\rm GATE}$ rises to high.

The time-to-voltage converter converts the pulsewidths of Q_1 and Q_2 to the voltage levels of $V_{T,H}$ and $V_{T,L}$ by charging storage capacitors (C_{ST1} and C_{ST2}) with constant reference currents (I_{REF1} and I_{REF2}), respectively.

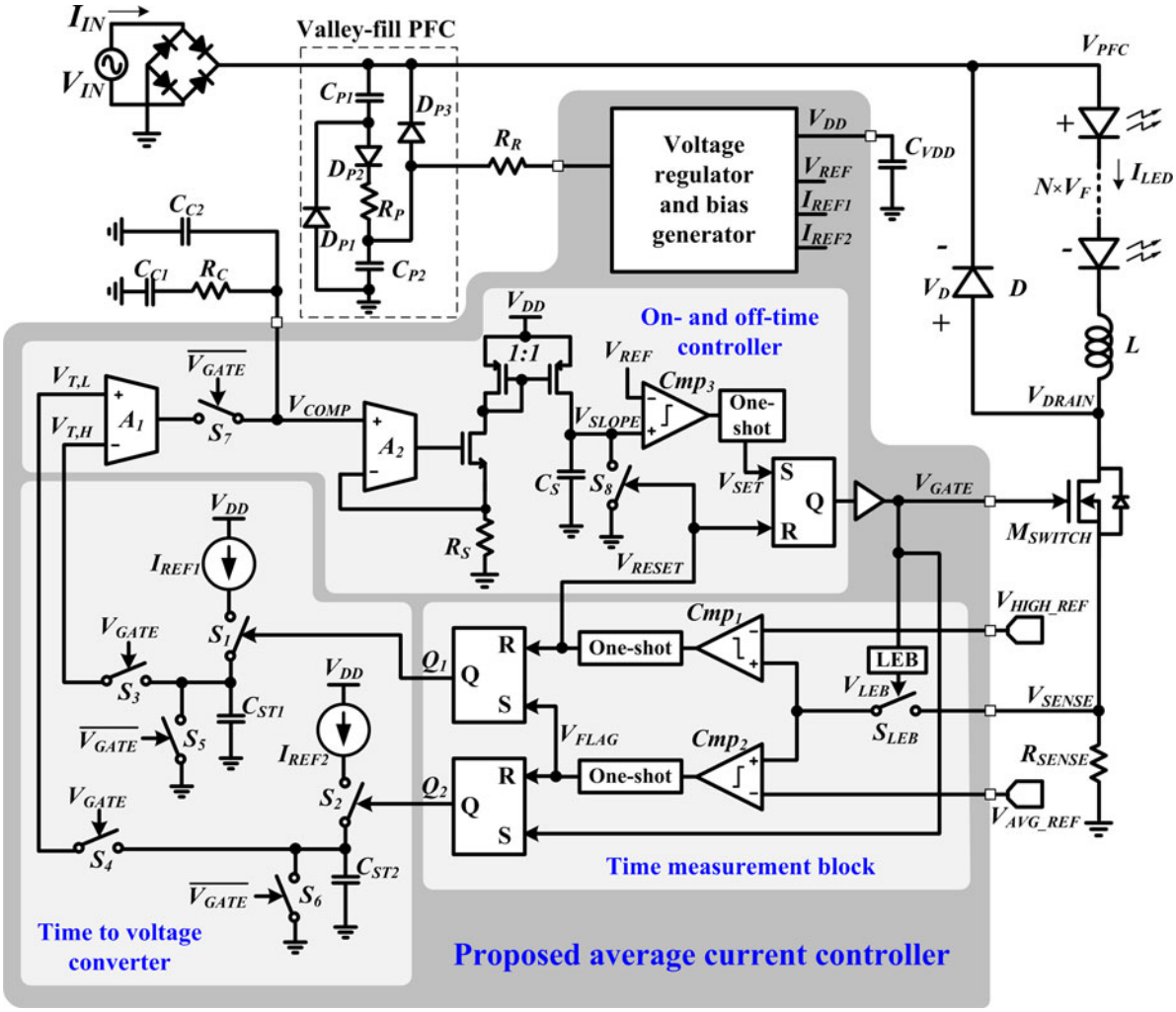

Fig. 5. Schematic of the proposed LED lamp driver with an average current controller.

The on- and off-time controller controls the charging current ($V_{\rm COMP}/R_S$) flowing into C_S by comparing $V_{T,H}$ and $V_{T,L}$ using the amplifiers (A_1 and A_2) and, thus, adjusts the time for a voltage across C_S ($V_{\rm SLOPE}$) to reach $V_{\rm REF}$. When $V_{\rm SLOPE}$ reaches $V_{\rm REF}$, the comparator ($\rm Cmp_3$) triggers $V_{\rm SET}$, and $V_{\rm GATE}$ is activated. Then, $M_{\rm SWITCH}$ is turned ON, and $I_{\rm LED}$ starts to increase, resulting in increasing $V_{\rm SENSE}$. When $V_{\rm SENSE}$ reaches $V_{\rm HIGH\_REF}$, the comparator ($\rm Cmp_1$) triggers $V_{\rm RESET}$, and $V_{\rm GATE}$ is deactivated, and then $M_{\rm SWITCH}$ is turned OFF. Thus, the on- and off-times of $M_{\rm SWITCH}$ are adjusted to generate the accurate average $I_{\rm LED}$.

The block for the voltage regulator and bias generator provides a supply voltage ($V_{\rm DD}$), a reference voltage ($V_{\rm REF}$), and reference currents (I_{REF1} and I_{REF2}) to the proposed average current controller.

The off-chip devices of C_{C1}, C_{C2}, and R_C are compensation components for the stable operation of the proposed LED lamp driver.

B. Valley-Fill PFC

The valley-fill PFC consists of two charging capacitors (C_{P1} and C_{P2}), three Schottky diodes (D_{P1}–D_{P3}), and a protection resistor (R_P) [26]. C_{P1} and C_{P2} are multiple-layer ceramic capacitors instead of electrolytic capacitors in order to reduce the system size and increase the lifetime of the LED lamp driver [13].

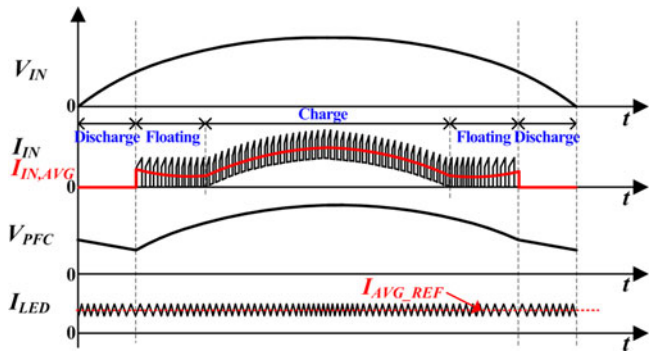

Fig. 6. Input and output waveforms of the proposed LED lamp driver using a valley-fill PFC.

Fig. 6 shows the waveforms of $V_{\rm PFC}$ and $I_{\rm LED}$ at the output of the valley-fill PFC according to $V_{\rm IN}$ and $I_{\rm IN}$. When $V_{\rm IN}$ is less than the voltage across C_{P1} and C_{P2} in parallel, the PFC supplies $V_{\rm PFC}$ and $I_{\rm LED}$ to the LEDs, and C_{P1} and C_{P2} are

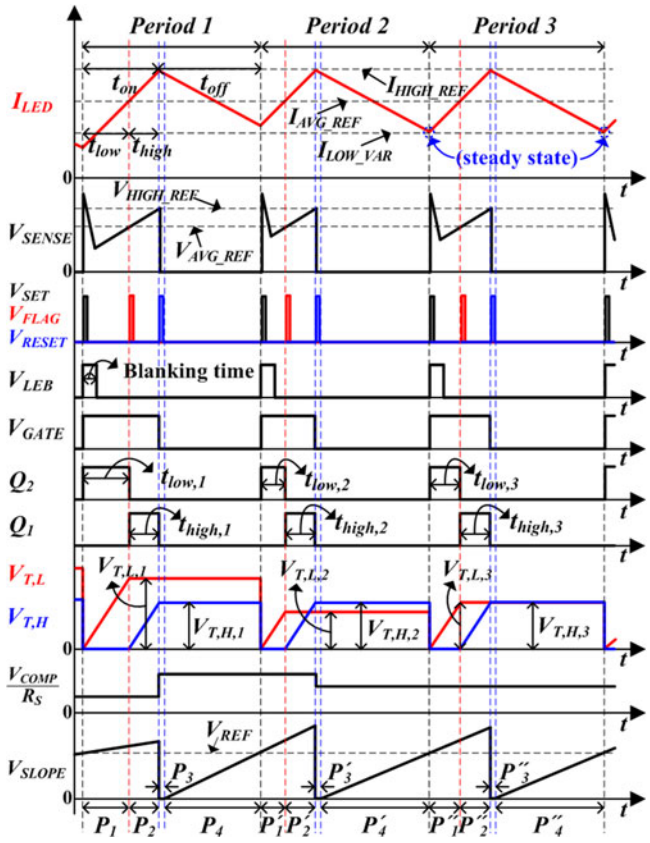

Fig. 7. Detailed waveforms of the LED lamp driver using the proposed ACC method.

then discharged (discharge phase). When V_{IN} is greater than the voltage across C_{P1} and C_{P2} in series, V_{IN} supplies V_{PFC} and I_{LED} to the LEDs, and C_{P1} and C_{P2} are then charged (charge phase). Except during the above discharge and charge phases, V_{IN} directly supplies V_{PFC} and I_{LED} to the LEDs, and C_{P1} and C_{P2} are floating (floating phase). Because the valley-fill PFC is used as a power buffer in the discharge phase, the average I_{LED} can be constantly regulated while maintaining the LEDs in the ON state. In addition, the PFC achieves a high power factor by keeping V_{IN} and $I_{IN,AVG}$ in-phase.

C. Operation of the Proposed Average Current Controller

Fig. 7 shows the detailed waveforms of the proposed LED lamp driver using the ACC method, depicting how the average I_{LED} is accurately controlled to I_{AVG_REF} by adjusting t_{on} and t_{off}. Each period represents one switching time of the proposed LED lamp driver, which consists of t_{on} and t_{off} and operates in four phases ($P_1 \sim P_4$ phases). t_{on} is divided into P_1 and P_2 phases for t_{low} and t_{high}, respectively. On the other hand, t_{off} is divided into P_3 and P_4 phases, in which C_S is discharged and the off-time of M_{SWITCH} is adjusted, respectively.

Fig. 8 shows the four operation phases of the proposed LED lamp driver in one switching period, corresponding to the waveform in Fig. 7.

As shown in Fig. 8(a) (P_1 phase), V_{SET} in the on- and off-time controller is triggered by Cmp_3 when V_{SLOPE} reaches V_{REF}. Then, it activates V_{GATE}, V_{LEB}, and Q_2. M_{SWITCH} is then turned ON, and I_{LED} begins to rise with a constant slope, as expressed in (2). Next, in the time-to-voltage converter, S_2 is turned ON as Q_2 is switched to the high state. Q_2 remains high for $t_{low,1}$, as shown in Fig. 7, until V_{SENSE} reaches V_{AVG_REF} in the time measurement block. During $t_{low,1}$, I_{REF2} charges C_{ST2}, and $V_{T,L,1}$ is stored in C_{ST2}, where $V_{T,L,1}$ is determined as

$$V_{T,L,1} = \frac{1}{C_{ST2}} \int_{\langle t_{low,1} \rangle} I_{REF2} dt. \tag{6}$$

As shown in Fig. 8(b) (P_2 phase), V_{FLAG} in the time measurement block is triggered by Cmp_2 when V_{SENSE} reaches V_{AVG_REF}. Then, it activates Q_1 and deactivates Q_2. Next, in the time-to-voltage converter, S_1 is turned ON as Q_1 is switched to the high state. Q_1 remains high for $t_{high,1}$, as shown in Fig. 7, until V_{SENSE} reaches V_{HIGH_REF} in the time measurement block. During $t_{high,1}$, I_{REF1} charges C_{ST1}, and $V_{T,H,1}$ is stored in C_{ST1}, where $V_{T,H,1}$ is determined as

$$V_{T,H,1} = \frac{1}{C_{ST1}} \int_{\langle t_{high,1} \rangle} I_{REF1} dt. \tag{7}$$

As shown in Fig. 8(c) (P_3 phase), V_{RESET} in the on- and off-time controller is triggered by Cmp_2 when V_{SENSE} reaches V_{HIGH_REF}. Then, it discharges C_S and deactivates V_{GATE} and Q_1. M_{SWITCH} is then turned OFF, and I_{LED} begins to decrease with a constant slope, as expressed in (3). Next, $V_{T,L,1}$ and $V_{T,H,1}$ are held at the input nodes of A_1 in the on- and off-time controller when S_3 and S_4 are turned OFF by V_{GATE}, respectively. C_{ST1} and C_{ST2} are then discharged when S_5 and S_6 are turned ON, respectively. Because the duration of $t_{low,1}$ is longer than that of $t_{high,1}$, $V_{T,L,1}$ is higher than $V_{T,H,1}$. Consequently, A_1 and A_2 increase the charging current in C_S (V_{COMP}/R_S) when S_7 is turned ON.

As shown in Fig. 8(d) (P_4 phase), V_{SLOPE} in the on- and off-time controller starts to rise by charging C_S with V_{COMP}/R_S when S_8 is turned OFF by V_{RESET}. M_{SWITCH} then remains turned OFF until V_{SLOPE} reaches V_{REF}. As V_{COMP}/R_S increases in the P_3 phase, the increasing rate of V_{SLOPE} increases, resulting in a decrease of the off-time of M_{SWITCH}.

The above four phases are repeated every switching period. In the next switching period (*Period* 2), from P'_1 to P'_3 phase, $V_{T,L,2}$ is determined to be lower than $V_{T,H,2}$, resulting in decreasing V_{COMP}/R_S. As the increasing rate of V_{SLOPE} decreases in phase P'_4, the off-time of M_{SWITCH} increases. In the same manner, from P''_1 to P''_3 phase, $V_{T,L,3}$ is determined to be equal to $V_{T,H,3}$, resulting in a constant and maintained V_{COMP}/R_S. As the increasing rate of V_{SLOPE} no longer varies in phase P''_4, the off-time of M_{SWITCH} remains unchanged. Consequently, the average I_{LED} is accurately regulated to I_{AVG_REF}, and the LED lamp driver finally operates in the steady state.

In the steady state, even when V_{PFC} varies to V'_{PFC} due to the variation in V_{IN} with a low frequency of 60 Hz, the proposed average current controller accurately controls I_{LED} in the same operation as described above, as shown in Fig. 9. During t_{on} at V'_{PFC} (t'_{on}), the slope of I'_{LED} varies as

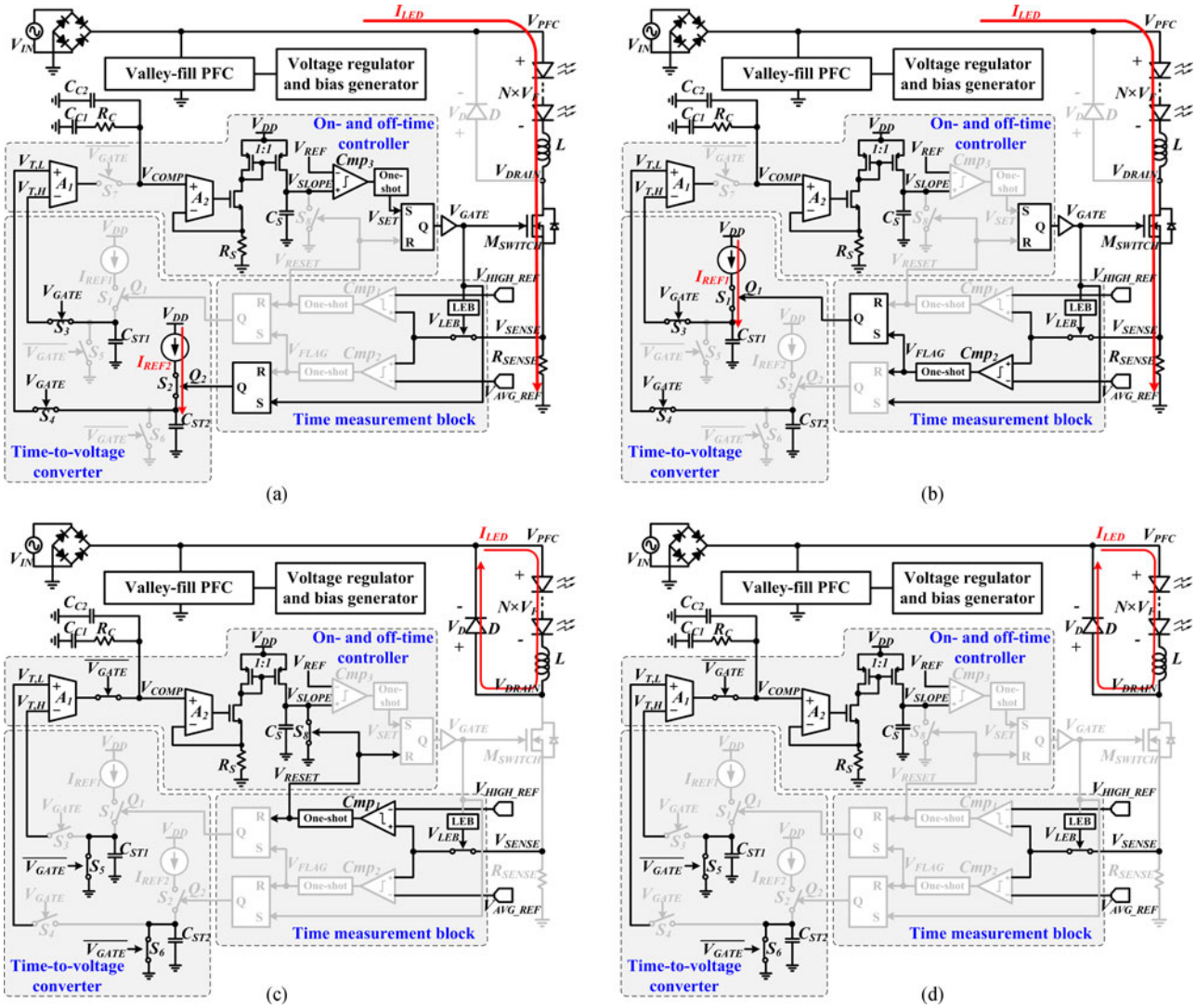

Fig. 8. Four operation phases of the proposed LED lamp driver: (a) P_1, (b) P_2, (c) P_3, and (d) P_4 phases.

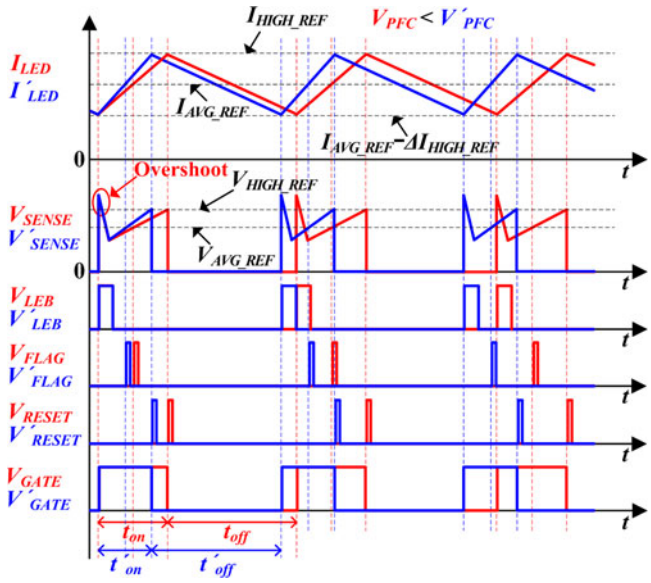

Fig. 9. Waveforms of the LED lamp driver when V_{PFC} varies in the steady state.

$$\frac{dI'_{\mathrm{LED}}}{dt'_{\mathrm{on}}} = \frac{V'_{\mathrm{PFC}} - N \times V_F - V_{\mathrm{DRAIN}}}{L}. \tag{8}$$

When V'_{SENSE} reaches $V_{\mathrm{AVG\_REF}}$ and $V_{\mathrm{HIGH\_REF}}$, V'_{FLAG} and V'_{RESET} are triggered, respectively, without being affected by V_{LEB}; therefore, the proposed controller can accurately control I_{LED} between $I_{\mathrm{HIGH\_REF}}$ and $I_{\mathrm{AVG\_REF}}$ minus ΔI_{HIGH}. Therefore, the low-frequency flicker can be removed regardless of the variation in V_{PFC}, which is caused by a varying V_{IN} with a low frequency of 60 Hz.

IV. Circuit Implementation of the LED Lamp Driver

This section presents how the key circuit elements in the proposed lamp driver are determined and implemented. The proposed LED lamp driver employs a structure of the floating buck converter with a valley-fill PFC to regulate I_{LED} with a high power factor for both 220 and 110 Vac of ac line voltage.

In the valley-fill PFC, the capacitance of both C_{P1} and C_{P2} is determined as

$$C_{\mathrm{PX}} = \frac{P_{\mathrm{OUT}} / V_{\mathrm{MIN}} \times t_{\mathrm{HOLD}}}{V_{\mathrm{DROP}}} \times \frac{1}{2}. \tag{9}$$

Here, P_{OUT} is a maximum output power of the LEDs, which is determined to be 12 W by considering a maximum $N \times V_F$ of 42 V and an $I_{\mathrm{AVG\_REF}}$ of 280 mA. V_{MIN} is the minimum voltage of V_{PFC}, which is determined to be 45 V by considering maximum $N \times V_F$ and voltage margin to drive M_{SWITCH}. t_{HOLD} is the holdup time for C_{P1} and C_{P2}, which is determined to be 2.7 ms by considering the valley region, which is one-third of the period of the rectified ac line voltage. V_{DROP} is the voltage drop on C_{P1} and C_{P2}, which is determined to be 25 V to ensure continuous conduction of LEDs. Thus, the capacitance of both C_{P1} and C_{P2} is determined to be 15 μF.

In the proposed LED lamp driver, the switching frequency adaptively varies according to V_{PFC}, $N \times V_F$, and ΔI, where ΔI is the current difference (current ripple) between the highest and lowest I_{LED}s in steady state, which can be expressed as

$$\Delta I = 2 \times (I_{\mathrm{HIGH\_REF}} - I_{\mathrm{AVG\_REF}}). \tag{10}$$

To avoid audible noise and consider the switching loss of M_{SWITCH}, the switching frequency is determined to be between 20 and 40 kHz. Thus, the switching period, which is the sum of t_{on} and t_{off}, is determined when satisfying the condition of $25\,\mu\mathrm{s} < t_{\mathrm{on}} + t_{\mathrm{off}} < 50\,\mu\mathrm{s}$. Here, t_{on} and t_{off} are, respectively, expressed as

$$t_{\mathrm{on}} = \frac{\Delta I \times L}{V_{\mathrm{PFC}} - N \times V_F - V_{\mathrm{DRAIN}}} \approx \frac{\Delta I \times L}{V_{\mathrm{PFC}} - N \times V_F} \tag{11}$$

and

$$t_{\mathrm{off}} = \frac{\Delta I \times L}{N \times V_F + V_D} \approx \frac{\Delta I \times L}{N \times V_F} \tag{12}$$

where V_{DRAIN} and V_D are a drain voltage of M_{SWITCH} and a forward voltage of freewheeling diode, which are negligibly small compared with V_{PFC} and $N \times V_F$, respectively. Therefore, $t_{\mathrm{on}} + t_{\mathrm{off}}$ can be determined as

$$t_{\mathrm{on}} + t_{\mathrm{off}} = \frac{\Delta I \times L \times V_{\mathrm{PFC}}}{(V_{\mathrm{PFC}} - N \times V_F) \times (N \times V_F)}. \tag{13}$$

The inductance can be derived from (13) as

$$L = \frac{(t_{\mathrm{on}} + t_{\mathrm{off}}) \times (V_{\mathrm{PFC}} - N \times V_F) \times (N \times V_F)}{\Delta I \times V_{\mathrm{PFC}}}. \tag{14}$$

Consequently, the inductance value is determined to be 6.8 mH using a nominal value of parameters in (14); 37.5 μs for $t_{\mathrm{on}} + t_{\mathrm{off}}$, 220 V for V_{PFC}, 34 V for $N \times V_F$, and 160 mA for ΔI. Here, to guarantee the above switching period range over the entire range of V_{PFC}, the nominal values of the switching period and V_{PFC} were selected to be 37.5 μs and 220 V, respectively. In addition, because the maximum percent flicker is determined to be 30%, the ripple current is selected to be 160 mA at an average I_{LED} of 280 mA (percentage flicker of 28.6%). To make a current ripple of 160 mA and an average I_{LED} of 280 mA, $V_{\mathrm{HIGH\_REF}}$, $V_{\mathrm{AVG\_REF}}$, and R_{SENSE} are designed to be 0.72 V, 0.56 V, and 2 Ω, respectively. On the other hand,

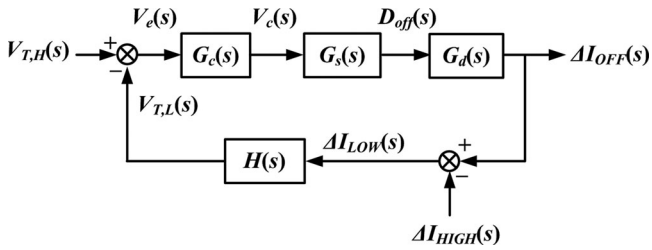

Fig. 10. Feedback loop of the proposed LED lamp driver.

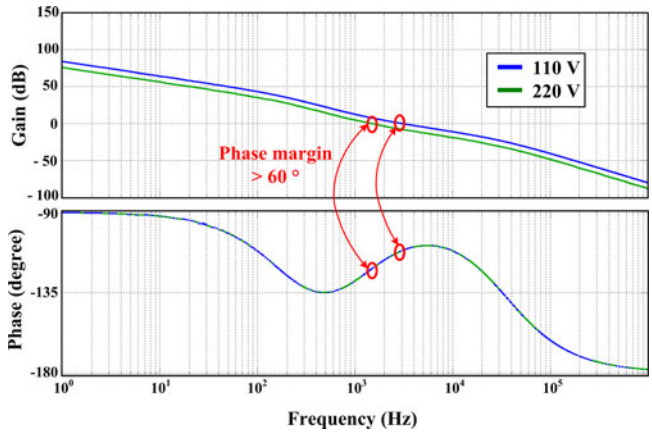

Fig. 11. Simulated loop response at different ac line voltage of 110 and 220 V.

when an ac line voltage of 110 Vac is used, the current ripple should be 80 mA to guarantee the above switching period range, and, thus, a $V_{\mathrm{HIGH\_REF}}$ of 0.64 V is used.

C_{ST1} and C_{ST2} in the time-to-voltage converter are designed to be 20 pF to stably hold $V_{T,H}$ and $V_{T,L}$, respectively, considering the area of the block. To charge C_{ST1} and C_{ST2} to a maximum voltage of 6 V for a maximum switching period of 50 μs, I_{REF1} and I_{REF2} are set to 2.4 μA. C_S in the on- and off-time controller is designed to be 20 pF considering the chip area and the operation range of V_{COMP}, which is set to be between 0.2 and 2.0 V. To make the proposed LED lamp driver properly operate at a switching frequency between 20 and 40 kHz, C_S should be charged to a V_{REF} of 3 V during the off-time duration of the proposed LED lamp driver between 4.5 and 45.0 μs. Thus, V_{COMP}/R_S should be between 1.3 and 13.3 μA. Consequently, R_S is determined to be 150 kΩ.

Fig. 10 shows the closed loop of the proposed LED driver, where $\Delta I_{\mathrm{OFF}}(s)$ is the current difference between the highest and lowest I_{LED}, $\Delta I_{\mathrm{HIGH}}(s)$ is the current difference between $I_{\mathrm{HIGH\_REF}}$ and $I_{\mathrm{AVG\_REF}}$, $V_e(s)$ is the error voltage between $V_{T,H}(s)$ and $V_{T,L}(s)$, $V_c(s)$ is the compensated voltage, and $D_{\mathrm{off}}(s)$ is the off-time duration of M_{SWITCH}, respectively, in the frequency domain. The loop gain $T(s)$ can be expressed as

$$T(s) = G_c(s) \cdot G_s(s) \cdot G_d(s) \cdot H(s) \tag{15}$$

where $G_c(s)$, $G_s(s)$, $G_d(s)$, and $H(s)$ are the transfer functions of a compensation network with amplifier, an off-time control network, a main switching network, and a feedback network,

TABLE I
DESIGN PARAMETERS OF THE LED LAMP DRIVER

Symbol	Description	Value (Part Number)
V_{IN}	input ac line voltage	110 V_{rms}, 220 V_{rms}
V_F	forward voltage of LED	2.8 V∼4.2 V
N	number of LEDs	5∼10 LEDs
I_{AVG_REF}	desired average current of LEDs	280 mA
I_{HIGH_REF}	peak current of LEDs	360 mA@220 V_{rms}, 320 mA@110 V_{rms}
I_{LOW}	lowest current of LEDs	200 mA@220 V_{rms}, 240 mA@110 V_{rms}
V_{AVG_REF}	reference voltage for I_{AVG_REF}	0.56 V
V_{HIGH_REF}	reference voltage for I_{HIGH_REF}	0.72 V@220 V_{rms}, 0.64 V@110 V_{rms}
L	inductance of buck converter	6.8 mH (19R685C)
V_{REF}	reference voltage for V_{SLOPE}	3 V
$I_{REF1,2}$	reference current for $V_{T,H}$ and $V_{T,L}$	2.4 μA
R_{SENSE}	resistance for sensing current	2 Ω (MBB02070C)
$C_{ST1,2}$	storage capacitance for $V_{T,H}$ and $V_{T,L}$	20 pF
C_S	capacitance for V_{SLOPE}	20 pF
R_S	resistance for V_{SLOPE}	150 kΩ
R_C	resistance for compensation	20 kΩ
$C_{C1,2}$	capacitance for compensation	1 nF and 30 nF
M_{SWITCH}	power MOSFET	(FQP11N40CF)
D	freewheeling diode	(SBR1U400P1-7)
$C_{P1,2}$	MLCC for PFC	15 μF (KTD251B156M99A0B00)
$D_{P1,2,3}$	diodes for PFC	(SBR1U400P1-7)

respectively. Each transfer function can be expressed as

$$G_c(s) = \frac{-g_m}{(1+s/\omega_p)} \cdot \frac{1+(C_{C1}\cdot R_C)s}{(C_{C1}+C_{C2})s+(C_{C1}\cdot C_{C2}\cdot R_C)s^2} \tag{16}$$

where g_m and ω_p are a transconductance of A_1 and frequency of pole in A_1, respectively

$$G_s(s) = -\frac{V_{\text{REF}}\cdot C_S\cdot R_S}{{V_{\text{COMP}}}^2} \tag{17}$$

$$G_d(s) = -\frac{N\cdot V_F}{L} \tag{18}$$

and

$$H(s) = \frac{L\cdot I_{\text{REF2}}}{(V_{\text{IN}}-N\cdot V_F)\cdot C_{\text{ST2}}}. \tag{19}$$

The Bode plots of $T(s)$ are depicted in Fig. 11 at different ac line voltages (V_{IN}s) to clearly show the stability of the proposed LED lamp driver. Both phase margins at 110 and 220 V ac are greater than 60°, indicating that the proposed LED lamp driver stably operates.

The design parameters and specifications of the proposed LED lamp driver are listed in Table I.

V. EXPERIMENTAL RESULTS

Fig. 12 shows the chip photomicrograph of the proposed average current controller fabricated using a 0.18 μm bipolar-CMOS-DMOS (BCD) process technology.

Fig. 13(a) and (b) shows the prototype of the proposed LED lamp driver and the ten LEDs lit up, respectively. In addition, Fig. 13(c) and (d) shows the enlarged photos of the valley-fill PFC and inductor, respectively. The capacitors (C_{P1} and C_{P2}) in the valley-fill PFC, both of which are made up of multilayer ceramic, have the same capacitance value and size of 15 μF

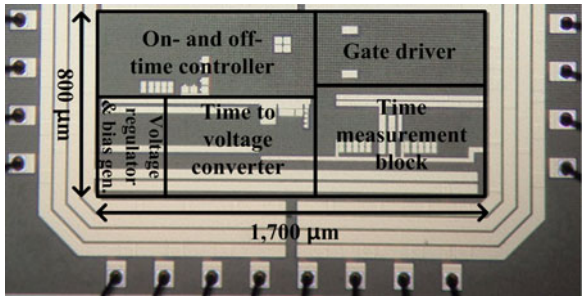

Fig. 12. Chip photomicrograph of the proposed average current controller.

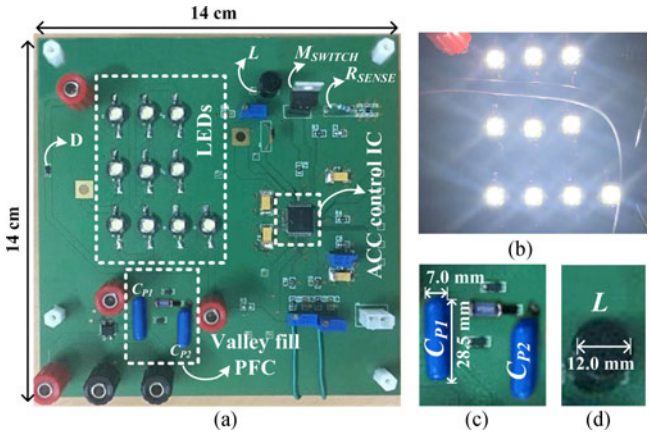

Fig. 13. (a) Prototype of the proposed LED lamp driver, (b) 10 LEDs lit up, (c) enlarged photo of valley-fill PFC, and (d) enlarged photo of inductor.

and 28.5 mm × 7.0 mm, respectively. The inductor (L) has an inductance value of 6.8 mH and a diameter of 12.0 mm.

Fig. 14 shows the measured waveforms of V_{PFC} and I_{LED} of the proposed LED lamp driver at an ac line voltage of 220 V_{rms}/60 Hz, an L of 6.8 mH, and an $N \times V_F$ of 35 V. The measurement results show that the lowest and highest levels of

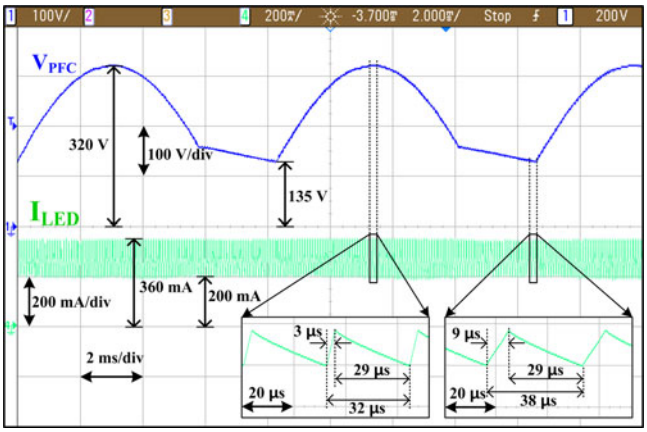

Fig. 14. Measured waveforms of V_{PFC} and I_{LED} when $L = 6.8$ mH and $N \times V_F = 34$ V.

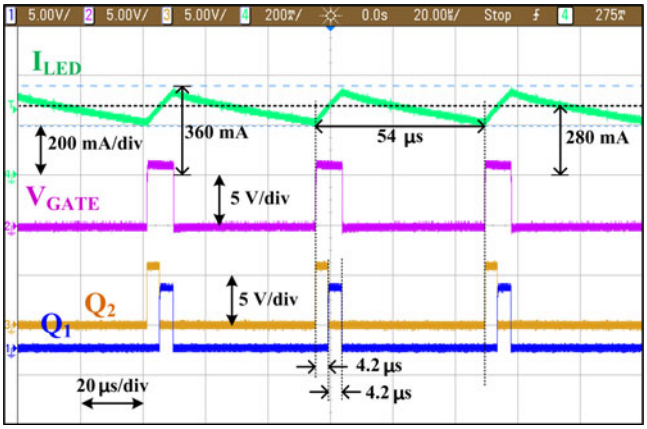

Fig. 15. Measured waveforms of I_{LED}, V_{GATE}, Q_1, and Q_2 when $L = 8.2$ mH and $N \times V_F = 28$ V.

I_{LED} are precisely regulated to be 200 and 360 mA, respectively, even when V_{PFC} varies from 135 to 320 V. The rising and falling times of I_{LED} are measured to be 3 and 29 μs at a V_{PFC} of 320 V, and 9 and 29 μs at a V_{PFC} of 135 V, respectively. Although V_{PFC} varies with 120 Hz, the proposed average current controller accurately controls the average I_{LED} to be 280 mA by adjusting the on-time of M_{SWITCH}; thus, the low-frequency (120 Hz) flicker is removed.

Fig. 15 shows the measured waveforms of I_{LED}, V_{GATE}, Q_1, and Q_2 when L is 8.2 mH and $N \times V_F$ is 28 V. The measurement results show that I_{LED} is hysteretically controlled from 200 to 360 mA at a switching period of 54 μs. When V_{GATE} is high (6 V) to turn ON M_{SWITCH}, I_{LED} starts to rise. During the rising time of I_{LED}, the pulsewidths of Q_1 and Q_2 are equally controlled to be 4.2 μs so as to regulate the average value of I_{LED} to be 280 mA.

Fig. 16(a) and (b) shows the measured waveforms of I_{LED}, V_{GATE}, and V_{SENSE} when L is 8.2 mH and $N \times V_F$ is 28 V, and when L is 6.8 mH and $N \times V_F$ is 28 V, respectively, indicating that the amplitude of I_{LED} and the switching frequency are 160 mA and 18.5 kHz and 160 mA and 22.7 kHz, respectively. The proposed average current controller adjusts the on- and off-time durations of the proposed LED lamp driver

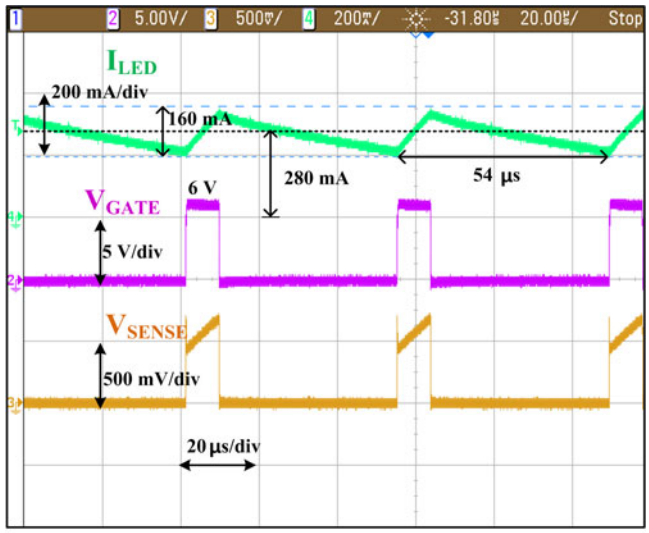

(a)

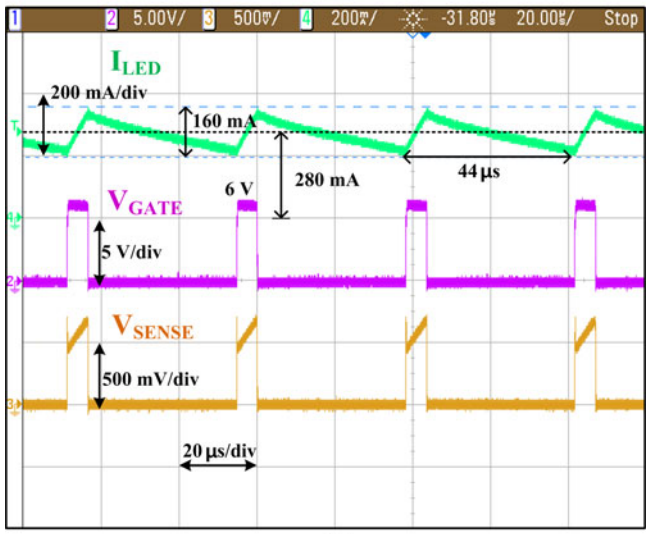

(b)

Fig. 16. Measured waveforms of I_{LED}, V_{GATE}, and V_{SENSE} when (a) $L = 8.2$ mH and $N \times V_F = 28$ V and (b) $L = 6.8$ mH and $N \times V_F = 28$ V.

to maintain the amplitude of I_{LED}. These results demonstrate that the LED lamp driver using the proposed average current controller maintains the same amplitude of I_{LED} regardless of the value of L, indicating that the proposed LED lamp driver accurately controls the luminance of LEDs.

Fig. 17 shows the transient response of I_{LED} when V_{IN} steps up from 0 V to 220 Vac. When V_{ENABLE}, which is an enable signal to turn ON the LED lamp driver, is turned ON, the system is activated, V_{IN} starts supplying power to the LED driver, and I_{LED} is then regulated to the target maximum and minimum current levels of 360 and 200 mA, respectively. When the proposed LED lamp driver operates in the turn on transient, the overshoot does not occur at the upper I_{LED} level since the maximum I_{LED} level is controlled by the comparator (Cmp_1 in Fig. 5). On the other hand, since the minimum I_{LED} level is controlled by amplifiers (A_1 and A_2 in Fig. 5) in the feedback network, a settling time for I_{LED} is needed to settle down to a target minimum current level. The required settling time of the minimum I_{LED} level to a target

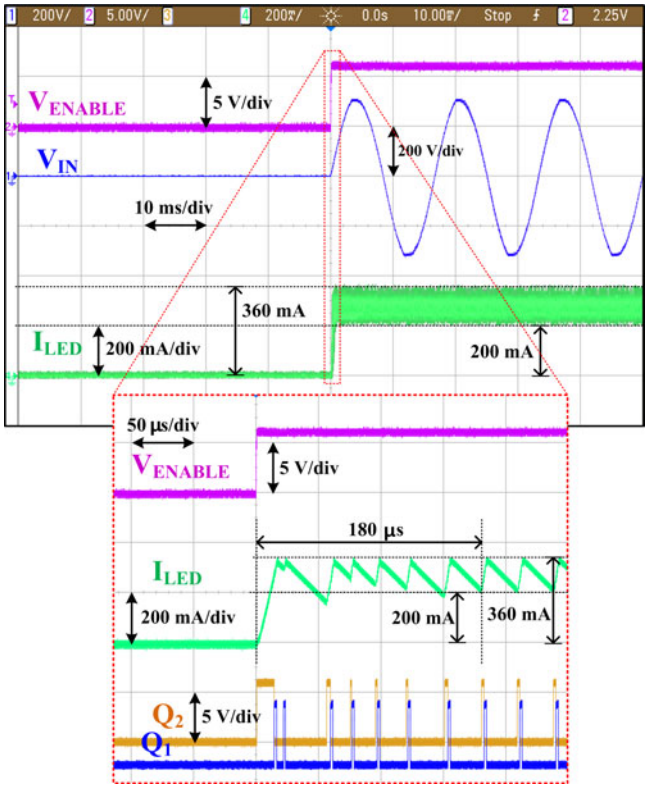

Fig. 17. Measured waveforms of the transient response of I_{LED} when V_{IN} steps up from 0 to 220 Vac and its zoomed-in area.

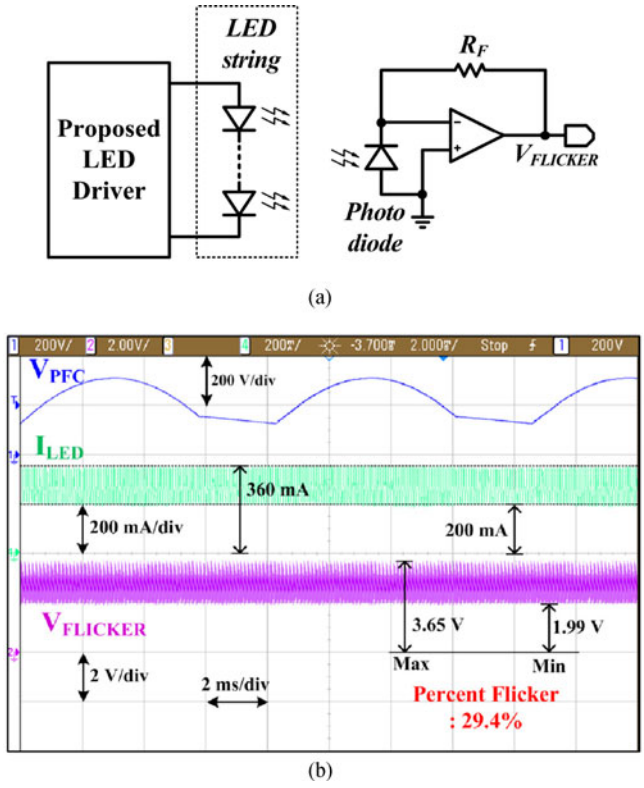

Fig. 18. (a) Test circuit for optical flicker and (b) measured waveform of flicker.

current level of 200 mA is 180 μs as shown in the zoomed-in area of Fig. 17.

Fig. 18(a) and (b) shows the test circuit for optical flicker and the measured waveform of flicker. To detect the light emitted from the LED string of the proposed LED driver, a photodiode was used to linearly convert the light of LEDs to the reverse current. In addition, an amplifier and a feedback resistor (R_F) were used to measure flicker as a voltage (V_{FLICKER}). The measured waveform of V_{FLICKER} showed that there remained only the high-frequency flicker while the low-frequency (120 Hz) flicker was removed by the proposed LED lamp driver. The maximum and minimum voltage levels of V_{FLICKER} are 3.65 and 1.99 V, respectively, resulting in a percent flicker of 29.4%. Fig. 19 indicates that the above measured percent flicker is satisfied with the IEEE standard 1789-2015 at the operation frequency range of the proposed LED lamp driver from 20 to 40 kHz.

Fig. 20(a) and (b) shows the measured waveforms of the ac input voltage (V_{IN}), input current (I_{IN}), V_{PFC}, and I_{LED} at 220 and 110 Vac, respectively. V_{IN} and I_{IN}, which are in phase, have the power factors of 0.91 and 0.93, respectively, while the average I_{LED} is constantly regulated to be 280 mA without low-frequency flicker.

Fig. 21 shows the average I_{LED} according to ac line voltage. The simulated average I_{LED} using the conventional AOT control method decreases, and its variation is 4.4%, whereas the measured average I_{LED} using the proposed ACC method has an almost constant value of 280 mA regardless of L value, and its variation is 0.6%.

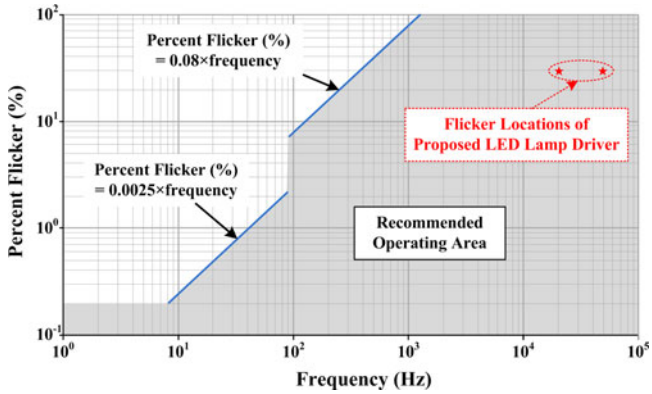

Fig. 19. Percent flicker locations of the proposed LED lamp driver according to frequency in the IEEE standard 1789-2015 [9].

Fig. 22 shows the power factor and power efficiency of the proposed LED lamp driver with respect to the number of LEDs. The measured maximum power factor and power efficiency are 0.93 and 89.22%, respectively. As the number of LEDs increases from 5 to 10 LEDs, the power efficiency increases. Since the off-time duration of the main switch decreases according to (12), the power consumption in the freewheeling diode decreases, which is the third largest power loss (1.97%) in the proposed LED lamp driver. On the other hand, as the number of LEDs increases over ten LEDs, the power efficiency decreases because the increments of the power consumption in the R_{SENSE} and on-resistance of M_{SWITCH} (R_{ON}) are larger than the decrement of the power consumption in the freewheeling diode. In addition,

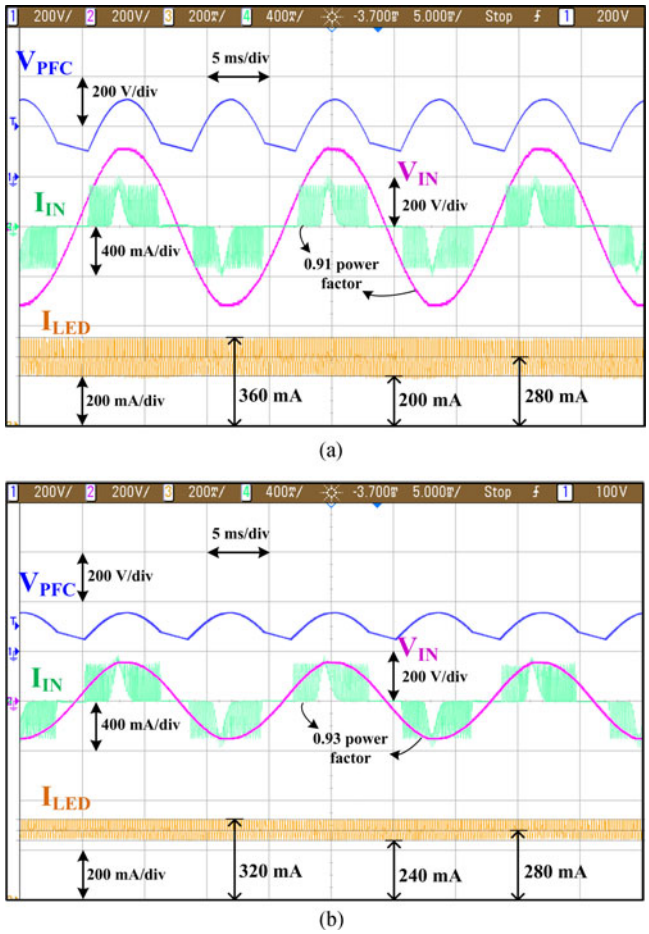

Fig. 20. Measured waveforms of V_{PFC}, V_{IN}, I_{IN}, and I_{LED} at (a) 220 Vac and (b) 110 Vac.

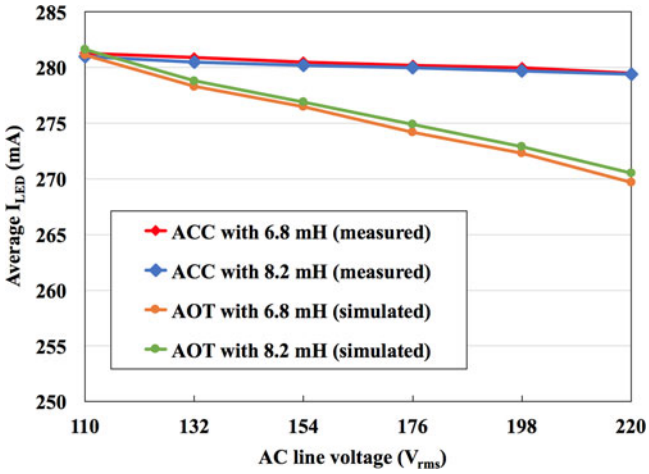

Fig. 21. Average I_{LED} according to ac line voltage and inductance.

as the ac line voltage increases, the on-time duration of the main switch decreases according to (11), and, thus, the power efficiency decreases. Also, as the number of LEDs increases, the power factor increases. Since the valley-fill PFC supplies more power when the ac line voltage is in the valley, the input current enables earlier charging of the capacitors in the valley-fill PFC. Thus, the shape of the input current becomes wider (close to a sinusoidal wave), resulting in an increase of the power factor. On the other hand, as the ac line voltage increases, the amount of current to charge the valley-fill PFC decreases, and thus the shape of the input current becomes narrower, resulting in a decrease of the power factor.

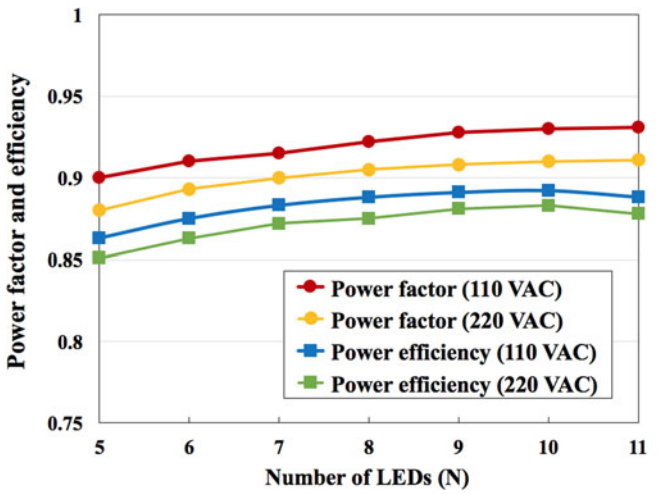

Fig. 22. Power factor and power efficiency of the proposed LED lamp driver using the ACC method with respect to the number of LEDs.

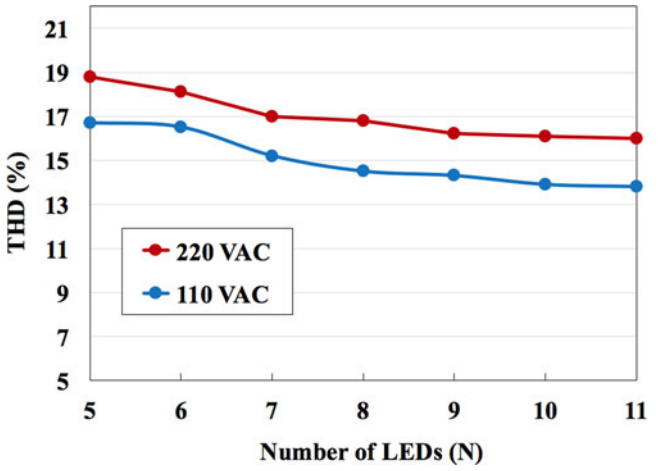

Fig. 23. THD according to the number of LEDs.

Fig. 23 shows the total harmonic distortion (THD) according to the number of LEDs, indicating that the proposed LED lamp driver satisfies the standard IEC 61000-3-2 at 110 and 220 V ac regardless of the number of LEDs since the THD is less than 19% [27]. As shown in Fig. 23, as the number of LEDs increases, the THD decreases due to an increase of power factor.

Fig. 24 shows the measured power breakdown of the proposed LED lamp driver; 89.22% for ten LEDs, 4.19% for inductor due to an equivalent serial resistance of 5.7 Ω, 2.51% for valley-fill PFC to store and supply power to the LEDs during the valley of the ac line voltage, 1.97% for the freewheeling diode due to a forward voltage of diode, and 1.72% for the proposed controller to charge and discharge the M_{SWITCH}'s gate capacitance of 1 nF. In addition, rectifier, R_{SENSE}, and on-resistance of M_{SWITCH} (R_{on}) consume 0.34, 0.04, and 0.01%, respectively.

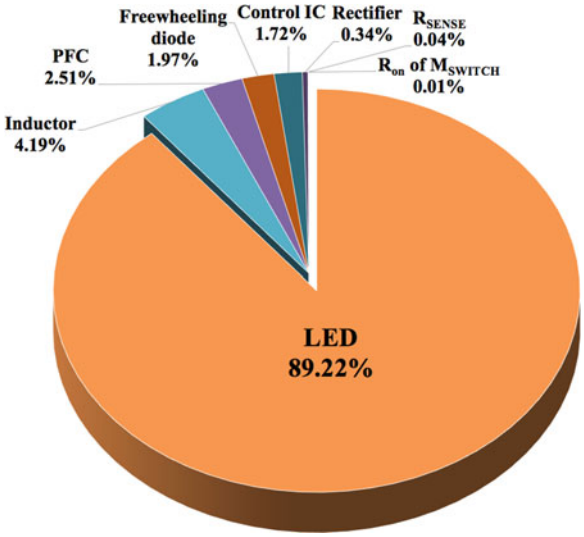

Fig. 24. Power breakdown of the proposed LED lamp driver.

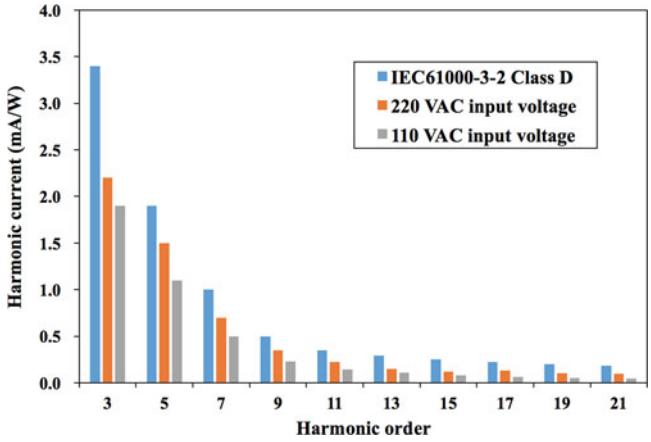

Fig. 25. Measured input current harmonics versus IEC 61000-3-2 Class D.

As shown in Fig. 25, the measured harmonic spectra of the input current at V_{IN}s of 110 ac and 220 ac were compared with the limits imposed by IEC 61000-3-2 Class D. The comparison results show that the input current harmonics are below the IEC 61000-3-2 Class D limits.

These measurement results show that the proposed LED lamp driver using the ACC method controls the luminance of LEDs with high current accuracy, high power factor, and without low-frequency flicker.

VI. Conclusion

An ACC method has been presented to achieve a highly accurate current for an LED lamp driver and to remove the low-frequency flicker. The proposed LED lamp driver adjusts the on- and off-times of the main power switch according to sensed information of I_{LED} and thus accurately controls I_{LED} without low-frequency flicker, regardless of variations in the ac input voltage, inductance, forward voltage of the LED, and the number of LEDs. In addition, the proposed LED lamp driver achieves high power efficiency with low system cost by controlling I_{LED} without a high-side resistor or a high-voltage sensor.

To verify the performance of the average current controller, the proposed LED lamp driver was designed and measured. The measurement results demonstrate that the proposed LED lamp driver using the ACC method has very little variation (less than 0.6%) in the average LED forward current. In addition, the measured maximum power efficiency and power factor are 89.22% and 0.93, respectively. The proposed LED driver has a little bit lower efficiency compared to traditional high efficient LED driver. However, the proposed LED driver has a simple structure having no bulky electrolytic capacitor, which is vulnerable to stress, and a smaller inductor instead of huge transformer, thus reducing the form factor. Moreover, the proposed ACC method achieves a highly accurate LED current with removal of low-frequency flicker regardless of variations in forward voltage of LEDs, inductance, and ac line voltage. Therefore, the proposed LED lamp driver is suitable for the high-quality lighting applications requiring low-cost and long lifetime.

References

[1] J. Y. Tsao, "Solid-state lighting: Lamps, chips, and materials for tomorrow," *IEEE Circuits Devices Mag.*, vol. 20, no. 3, pp. 28–37, Jun. 2004.

[2] D. G. Lamar, M. Arias, A. Rodriguez, A. Fernandez, M. M. Hernando, and J. Sebastian, "Design-oriented analysis and performance evaluation of a low-cost high-brightness LED driver based on flyback power factor corrector," *IEEE Trans. Ind. Electron.*, vol. 60, no. 7, pp. 2614–2626, Jun. 2013.

[3] Y. C. Li and C. L. Chen, "A novel single-stage high-power-factor ac-to-dc LED driving circuit with leakage inductance energy recycling," *IEEE Trans. Ind. Electron.*, vol. 59, no. 2, pp. 793–802, Feb. 2012.

[4] C. Moo, Y. Chen, and W. Yang, "An efficient driver for dimmable LED lighting," *IEEE Trans. Power Electron.*, vol. 27, no. 11, pp. 4613–4618, Nov. 2012.

[5] J. Veitch and S. McColl, "Modulation of fluorescent light: Flicker rate and light source effects on visual performance and visual comfort," *Light. Res. Technol.*, vol. 27, no. 4, pp. 243–256, Apr. 1995.

[6] L. Peretto, E. Pivello, R. Tinarelli, and A. E. Emanuel, "Theoretical analysis of the physiologic mechanism of luminous variation in eye–brain system," *IEEE Trans. Instrum. Meas.*, vol. 56, no. 1, pp. 164–170, Feb. 2007.

[7] A. Wilkins, J. Veitch, and B. Lehman, "LED lighting flicker and potential health concerns: IEEE standard PAR1789 update," in *Proc. IEEE Energy Convers. Congr. Expo*, 2010, pp. 171–178.

[8] B. Lehman, A. Wilkins, S. Berman, M. Poplawski, and N. J. Miller, "Proposing measures of flicker in the low frequencies for lighting applications," in *Proc. IEEE Energy Convers. Congr. Expo*, 2011, pp. 2865–2872.

[9] *IEEE Recommended Practices for Modulating Current in High-Brightness LEDs for Mitigating Health Risks to Viewers*, IEEE Standard 1789-2015, Jun. 2015.

[10] Y. Yang, X. Ruan, L. Zhang, J. He, and Z. Ye, "Feed-forward scheme for an electrolytic capacitor-less AC/DC LED driver to reduce output current ripple," *IEEE Trans. Power Electron.*, vol. 29, no. 10, pp. 5508–5517, Oct. 2014.

[11] J. C. W. Lam and P. K. Jain, "A high power factor, electrolytic capacitor-less AC-input LED driver topology with high frequency pulsating output current," *IEEE Trans. Power Electron.*, vol. 30, no. 2, pp. 943–955, Feb. 2015.

[12] P. Fang and Y. F. Liu, "Energy channeling LED driver technology to achieve flicker-free operation with true single stage power factor correction," *IEEE Trans. Power Electron.*, vol. 32, no. 5, pp. 3892–3907, May 2017.

[13] Y. Gao, L. Li, and P. K. T. Mok, "An AC input switching-converter-free LED driver with low-frequency-flicker reduction," *IEEE J. Solid-State Circuits*, vol. 52, no. 5, pp. 1424–1434, May 2017.

[14] H. C. Kim, M. C. Choi, S. Kim, and D. K. Jeong, "An AC–DC LED driver with a two-parallel inverted buck topology for reducing the light flicker in lighting applications to low-risk levels," *IEEE Trans. Power Electron.*, vol. 32, no. 5, pp. 3879–3891, May 2017.

[15] G. G. Pereira, M. A. Dalla Costa, J. M. Alonso, M. F. De Melo, and C. H. Barriquello, "LED driver based on input current shaper without electrolytic capacitor," *IEEE Trans. Ind. Electron.*, vol. 64, no. 6, pp. 4520–4529, Jun. 2017.
[16] S. Wang, X. Ruan, K. Yao, S. C. Tan, Y. Yang, and Z. Ye, "A flicker-free electrolytic capacitor-less AC–DC LED driver," *IEEE Trans. Power Electron.*, vol. 27, no. 11, pp. 4540–4548, Nov. 2012.
[17] P. S. Almeida, G. M. Soares, and H. A. C. Braga, "Off-line flyback LED driver with PWM dimming and power factor correction employing a single switch," in *Proc. 10th IEEE/IAS Int. Conf. Ind. Appl.*, Fortaleza, Brazil, 2012, pp. 1–7.
[18] S. Li, Y. Guo, S. C. Tan, and S. Y. Hui, "An off-line single-inductor multiple-output LED driver with high dimming precision and full dimming range," *IEEE Trans. Power Electron.*, vol. 32, no. 6, pp. 4716–4727, Jun. 2017.
[19] S. C. Hsia, S. Y. Lai, and J. J. Ciou, "High-power led dimming driver with multi-level current for smart street lighting system," in *Proc. Spec. Semin. Energy Efficient Green Netw.*, Riccarton, New Zealand, 2013, pp. 56–60.
[20] A. T. L. Lee, J. K. O. Sin, and P. C. H. Chan, "Scalability of quasi-hysteretic FSM-based digitally controlled single-inductor dual-string buck LED driver to multiple strings," *IEEE Trans. Power Electron.*, vol. 29, no. 1, pp. 501–513, Jan. 2014.
[21] M. G. Kim, "Error amplifier design of peak current controlled (PCC) buck LED driver," *IEEE Trans. Power Electron.*, vol. 29, no. 12, pp. 6789–6795, Dec. 2014.
[22] J. T. Hwang, K. Cho, D. Kim, M. Jung, G. Cho, and S. Yang, "A simple LED lamp driver IC with intelligent power-factor correction," in *Proc. IEEE Int. Solid-State Circuits Conf.*, San Francisco, CA, USA, 2011, pp. 236–238.
[23] S. Uprety, H. Chen, and D. Ma, "Quasi-hysteretic floating buck LED driver with adaptive off-time for accurate average current control in high brightness lighting," in *Proc. IEEE Int. Symp. Circuits Syst.*, Rio de Janeiro, Brazil, 2011, pp. 2893–2896.
[24] H. Deng, L. Shan, Y. Yin, G. Si, and Y. Sun, "Design of a LED constant-current driver using a novel hysteresis-current control method with adaptive off-time control," in *Proc. 8th Int. Congr. Image Signal Process.*, Shenyang, China, 2015, pp. 1551–1555.
[25] C. Shin *et al.*, "A sine-reference band (SRB)-controlled average current technique for a phase-cut dimmable AC-DC buck LED driver without an electrolytic capacitor," in *Proc. IEEE Symp. VLSI Technol.*, Honolulu, HI, USA, 2016, pp. 1–2.
[26] J. C. W. Lam, S. Pan, and P. K. Jain, "A single-switch valley-fill power-factor-corrected electronic ballast for compact fluorescent lightings with improved lamp current crest factor," *IEEE Trans. Ind. Electron.*, vol. 61, no. 9, pp. 4654–4664, Sep. 2014.
[27] Electromagnetic compatibility, Part 3, Section 2. Limits for Harmonic Current Emissions (Equipment Input Current $\leq$ 16 A Per Phase), IEC Standard 61000-3-2, 2005.

Hyun-A Ahn (S'12) received the B.S. degree in electrical and computer engineering in 2009 from Hanyang University, Seoul, South Korea, where he is currently working toward the Ph.D. degree in electronics and computer engineering at Hanyang University.

His research interests include power management IC design, LED lamp driver IC design, and micro-LED display driver IC design.

Seong-Kwan Hong (M'13) received the B.S. degree in electronic engineering from Hanyang University, Seoul, South Korea, in 1980, and the M.S. and Ph.D. degrees in electrical engineering from the Georgia Institute of Technology, Atlanta, GA, USA, in 1985 and 1994, respectively.

From 1990 to 1995, he was with Cadence Design Systems, Inc., San Jose, USA, where he developed several ECAD products. In 1995, he joined R&D Lab of LG Semicon, Seoul, where he was in charge of the Design Technology Center as a Research Fellow. In 1999, he became the Vice President and Chief Information Officer at Hynix Semiconductor, Inc., where he was responsible for the information technology and R&D engineering support. From 2009 to 2013, he was with Yonsei University, Seoul, as a Hynix Chair & Research Professor. In 2013, he joined Hanyang University as a Research Professor. His research interests include the area of EDA design methodology, mixed IC design, and automotive IC design.

Oh-Kyong Kwon (S'83–M'88) received the B.S. degree in electronic engineering from Hanyang University, Seoul, South Korea, in 1978, and the M.S. and Ph.D. degrees in electrical engineering from Stanford University, Stanford, CA, USA, in 1986 and 1988, respectively.

From 1987 to 1992, he was with the Semiconductor Process and Design Center, Texas Instruments Inc., Dallas, TX, USA, where he was working on the development of multichip module technologies and smart power integrated circuit technologies for automotive and flat panel display applications. In 1992, he joined Hanyang University as an Assistant Professor with the Department of Electronic Engineering and is currently a Professor with the Department of Electronic Engineering. He has authored and coauthored more than 353 international journal and conference papers and 237 U.S. patents. His research interests include capacitive touch systems, smart power integrated circuit technologies, mixed mode signal circuit design, imager, analog front-end circuit design for biomedical instruments, the driving methods and circuits for flat panel displays, interconnect and electrical noise modeling for high-speed system-level integration, and wafer-scale chip-size packages.